SPH Modeling and Investigation of the Shear and Blender Mixers for Mixing Cement Paste

Shamsoddini, Rahim*[+]

Department of Mechanical Engineering, Sirjan University of Technology, Sirjan, I.R. IRAN

Abolpour, Bahador

Department of Chemical Engineering, Sirjan University of Technology, Sirjan, I.R. IRAN

ABSTRACT: *Mixing and homogenization of cement paste are some of the most used phenomena in the construction and building industries. In most cases, a homogeneous mixture of cement paste is required and this is supplied by rotary mixers. In the present study, the rotary cement paste mixers in two-dimensional (2D) conditions are investigated by an Incompressible Smoothed Particle Hydrodynamics (ISPH) method. The method is validated and then used to model the cement paste mixer. The cement paste is considered a Bingham fluid. Two types of mixers are examined; shear mixer and blender. An appropriate mixing index that was previously applied to the discrete element method was successfully implemented for the ISPH method, and the performance of these two types of mixers is analyzed with this mixing index. The results show that the Reynolds number has a key role in the mixing in the shear mixers. In the low Reynolds numbers, an unmixed region is formed, which decreases with increasing Reynolds numbers. In blender mixers, the mixing rate is expected to increase with the multiplicity of vortices formed. But the coordinated motion of the vortices with the blades causes a fluid mass to move. Also, the resistance of the fluid to the moving components of the mixer is calculated and the difference in the performance of the two mixers in terms of energy consumption and mixing speed is compared and discussed.*

KEYWORDS: *Cement paste; SPH; Shear mixer; Blendr mixer; Resistant torque.*

INTRODUCTION

Fluid mixing is one of the most important processes in the chemical industry. Combined systems can include fluid mixing with any of the other phases: liquid, solid, and gas. Mixing operations can be used to mix a volume of fluid, chemical reaction, heat transfer, mass transfer, or multi-phase blend (suspension) in the industry. The mixing action can be accompanied by a disturbance in the liquid. This is called mixing and can be done by an external force or a blade-like device. By applying tangential blades, the blades rotate and create a vortex in the fluid that will eventually drive the mixing to a uniform composition. Mixing is a transition process for components, temperatures, and phases to reduce inhomogeneity.

Nowadays, to build a building, modern equipment and tools may be seen, each of which can facilitate the work and reduce manpower, and of course add more quality and

***** *To whom correspondence should be addressed.*
+ *E-mail: Shamsoddini@sirjantech.ac.ir*
1021-9986/2022/5/3181-3194 *14/$/5.04*

efficiency during the construction process. One of these equipment is cement mixers and cement mixture mixers. These mixers include Betoniera mixers and concrete trucks, which are added to their variety every day. The mixing technology of these mixers often includes shear mixing, blending mixing, or a combination of them.

Traditional numerical methods for following the mixing path include Eulerian-Eulerian methods and Eulerian-Lagrangian methods. The Eulerian-Eulerian method considers both phases in continuous environments, and the details of the concentration field are calculated using the survival equation. The accuracy of the Eulerian-Eulerian method depends heavily on the empirical survival equation. Besides, this method has limitations in predicting some disrupted flow properties. The Eulerian-Lagrangian analysis environment consists of a continuous (Eulerian) and a discrete (Lagrangian) environment. Eulerian-Lagrangian methods are usually multi-stage and are complex numerical methods and require high computational power and time [1].

Recently, fully Lagrangian methods have been introduced in the field of mixing flow modeling, which are generally based on particle methods. These methods also have many limitations. One of the most primitive particle methods is the Smoothed Particle Hydrodynamics (SPH). For the first time, *Gingold* and *Manahan* [2] and *Lucy* [3] used SPH to model astronomical phenomena. SPH has gradually expanded for fluid and solids mechanics problems.

SPH is now used to solve complex problems such as free-surface flow [4-7] multi-phase flows [8, 9], and fluid-solid interaction [11-14]. SPH has recently been applied for cement and concrete flows [15, 16]. It has also been used to simulate mixing flows [17-19]. But none of these works provided a good criterion for evaluating the mixing process. However, in some researches proper mixing index has been applied*; Shamsoddini et al.* [20] investigated the micromixing phenomenon in an active micromixer consisting of a microchannel in which a stirrer rotates to mix the fluid. They also studied the micromixing phenomena in a cylindrical paddle mixer using a modified weakly compressible SPH method (WCSPH) [21]. Other studies have also been done in this regard: mixing with two-blade [22], mixing in a tank with the free surface [23], and the rotary micropump mixer modeling [24]. *Abdolahzadeh et al.* [25] in a siresearchmilar work simulated the mixing process in circular and elliptical one-blade and two-blade blenders using the SPH method. All of the mentioned studies are for the miscible fluids and the mixing indices used in these works have been based on the concentration equation (Fick's second law).

Recently, several studies have been conducted on the physical properties of cement and its additives [26, 27]. The physical properties of cement are complex functions of different effective factors such as its blend, chemical properties, and extra [27]. *Lee* and *Choi* [28] proposed a mixing ratio for standard reference materials that can simulate the flow characteristics of cement paste, according to the water–cement ratio. *Li et al.* [29] fitted the rheological properties of fresh cement paste with different amounts of ultrafine circulating fluidized bed fly ash through the rheological models. The cement paste was considered a Bingham fluid.

There are very few numerical works in the field of modeling cement mixers, all of which have been done using mesh-based methods. *Shuiping et al.* [30] simulated and analyzed the flow field of a cement mixer based on numerical simulation with Fluent software. Using Ansys CFX, *Beccati et al.* [31] examined the influence of the viscosity model on the simulations of a drum mixer truck. However, in this study, the cement paste mixer is modeled by the SPH method. The most important purpose of the present study is to investigate and compare shear and blender mixers in terms of performance (mixing rate) and energy consumption. To evaluate the mixing rate, a mixing index is used which measures the mixing rate of two fluids without solving the concentration equation. This index indicates the degree of homogeneity of the components. This mixing index, first, was introduced by *Asmar et al.* [32] who model the mixing processes by Discrete Element Model (DEM). In the present study, to the best of our knowledge for the first time, this mixing index was defined and implemented in an SPH algorithm. To evaluate the power consumption, the fluid torque against the blade movement is calculated.

In the following, first, the governing equations and the solution algorithm are discussed, and then the results are investigated.

THEORETICAL SECTION

Numerical procedure

The formulation of SPH is based on the integral form, which shows that each continuous function f in the domain Ω is expressed as:

$$f(r) = \int_{\Omega} f(r')W(r - r')dr' \quad (1)$$

Where *r* and *r* ' are respectively position vector and integrating variable, *W* is the weight or kernel function, and *h* is the smoothing length. This equation is approximated by a numerical summation of discrete particles in the domain Ω:

$$f(r) = \sum_{j} \forall_j f_j W(r - r_j, h) \quad (2)$$

$\forall j$ is the volume of the particle j. In this study, the fifth-order Wendland kernel function is used. Using this kernel function increases the accuracy of fluid flow modeling [33]:

$$W(r,h) = \quad (3)$$
$$W_0 \times \begin{cases} \left(1 - \frac{|r|}{h}\right)^4 \left(4\frac{|r|}{h} + 1\right) & 0 \le \frac{|r|}{h} < 1 \\ 0 & \frac{|r|}{h} \ge 1 \end{cases}$$

W_0 is equal to $7 / \pi h^2$ in two-dimensional cases. The gradient, divergence, and Laplacian operator SPH discretizations which are used in the present study are as follows (*f* is an arbitrary scaler function and $\boldsymbol{F}$ is a tensor arbitrary function) :

$$\langle \nabla f \rangle_i = \sum_j \forall_j (f_j - f_i) B_i \cdot \nabla W_{ij} \quad (4)$$

$$\langle \nabla . F \rangle_i = \sum_j \forall_j (F_j - F_i) \cdot (B_i \cdot \nabla W_{ij}) \quad (5)$$

$$\langle \nabla^2 f \rangle_i = \sum_j \forall_j \left(\frac{f_j - f_i}{r_{ij}}\right) e_{ij} \cdot (B_i \cdot \nabla W_{ij}) \quad (6)$$

The governing equations include the mass and momentum continuity equations as follows:

$$\frac{1}{\rho}\frac{D\rho}{Dt} + \nabla \cdot V = 0 \quad (7)$$

$$\frac{DV}{Dt} = -\frac{1}{\rho}\nabla p + g + \frac{1}{\rho}\nabla . \tau \quad (8)$$

Where ρ is the density of each particle of the fluid, *t* is time, *V* is the velocity vector of the particle, *p* is pressure, *g* is the gravity acceleration, and $\boldsymbol{\tau}$ is the total shear stress tensor.

The present method is based on a predictive-corrective predictor. In the predictive step, the Poisson pressure equation is solved using the mean velocity: $\boldsymbol{V}_i^{*,n+1}$. The mean velocity is the velocity calculated according to the viscous and gravitational accelerations of the momentum equation:

$$V_i^{*,n+1} = V_i^n + \quad (9)$$
$$(g + \sum_j 2\forall_j(v_e)\frac{V_i - V_j}{r_{ij}} e_{ij} \cdot (B_i . \nabla W_{ij}))\Delta t$$

That is, $\forall_j$ is the volume of the particle j, e_{ij} is the unit vector (from the particle j to the particle i), $v_e = \mu_e/\rho$, and B_i is the correction tensor for the kernel function gradient [34]:

$$B_i = -\left[\sum_j \forall_j r_{ij} \nabla W_{ij}\right]^{-1} \quad (10)$$

The cement paste has non-Newtonian behaviour [35]. In the present study, the liquid behavior is modeled by the Bingham non-Newtonian fluid. In the Bingham model, the fluid resists inferiority to the shear stress. When the surrender tension goes beyond the limits, the flow structure changes and has behavioral properties such as Newtonian flu. When the shear stress falls below the yield stress, the fluid structure changes again. So, the shear stress of Bingham fluid is defined as follow:

$$\begin{cases} \tau = \left(\mu_0 + \frac{\tau_0}{\dot{\gamma}}\right)\dot{\gamma} & (\tau > \tau_0) \\ \dot{\gamma} = 0 & (\tau < \tau_{0)} \end{cases} \quad (11)$$

In the present study, to have a robust behavior, the regularized model presented by Papanastasiou [36] is used. So the stress tensor and effective viscosity are calculated by:

$$\tau = \mu_e \dot{\gamma} \quad (12)$$

$$\mu_e = \mu_0 + (\frac{\tau_0}{\dot{\gamma}})(1 - e^{-m\dot{\gamma}}) \quad (13)$$

Where τ_0 and μ_0 are respectively the yield stress and Bingham fluid viscosity and *m* is the regularization parameter. It is easy to prove that the Papanastasiou model is the same as the Bingham model when *m* tends to infinity [36]. So, in the present study, it is considered $m=10^6$. In two-dimensional problems, the strain rate tensor ($\dot{\boldsymbol{\gamma}}$) and value ($\dot{\gamma}$) is calculated as follows:

$$\dot{\gamma} = \nabla u + (\nabla u)^T \qquad \dot{\gamma} = \sqrt{\frac{1}{2}(\dot{\gamma}:\dot{\gamma})} \tag{14}$$

Based on the Poisson pressure equation, the pressure is calculated as follows:

$$\sum_j 2\frac{\forall_j}{\rho_{ij}}\frac{P_i^{n+1}-P_j^n}{r_{ij}}e_{ij}.\left(B_i.\nabla W_{ij}\right) = \frac{\langle \nabla \cdot V_i^{*,n+1}\rangle}{\Delta t} \tag{15}$$

After the calculation of the pressure, the velocity is corrected as follow:

$$V_i^{n+1} = V_i^{*,n+1} - \langle\frac{\nabla p}{\rho}\rangle_i^{n+1}\Delta t \tag{16}$$

Finally, the new position for all particles is calculated:

$$r_i^{n+1} = r_i^n + V_i^{n+1}\Delta t \tag{17}$$

Beside each wall boundary, two dummy particles rows are arranged. The velocity of each dummy particle is obtained by its corresponding wall particle. If the wall has linear motion with no acceleration, the velocity of the dummy particle is the same as its corresponding wall particle. For dummy particles, the pressure equation is achieved by dot multiplying the surface normal vector ($\boldsymbol{n}_w$) by the momentum equation:

$$\left(\frac{\nabla p}{\rho}\right)\cdot n_w = \frac{1}{\rho}\frac{\partial p}{\partial n_w} \tag{18}$$
$$= -\frac{dV_b}{dt}\cdot n_w + \left(\nabla\cdot(\nu_e\nabla V)\right)\cdot n_w + g.n_w$$

Whereas the dummy particles are fixed relative to the wall particles, this equation can be discretized by the Finite Difference Method:

$$p_i^{n+1} = p_i^n + \tag{19}$$
$$\rho\delta_n\left(-\frac{dV_b}{dt}\cdot n_w + \left(\nabla\cdot(\nu_e\nabla V)\right)\cdot n_w + g.n_w\right)$$

Failure, cluster alignment, and particle bonding are the inherent disadvantages of the SPH method. Particle shifting is a remedy for these unwanted phenomena. One of the pioneering works that introduced the shifting particle algorithm is the work of *Shadloo et al.* [37]. To prevent the occurrence of these unpleasant phenomena, a particle shifting algorithm similar to that reported by *Sefid et al.* [38] is implemented; the shifting vector is first calculated by:

$$\Delta r_i = \varepsilon\bar{r}_i \tag{19}$$

where ε is a constant factor between 0 and 0.1and $\bar{\boldsymbol{r}}_{\boldsymbol{i}}$ is:

$$\bar{r}_i = \sum_j \forall_j r_{ij} W_{ij} \tag{21}$$

Then the particle is shifted by $\Delta\boldsymbol{r}_{\boldsymbol{i}}$, the flow filed variables are corrected as follows:

$$V_i = V_i + \Delta V_i = V_i + \Delta r_i\cdot\langle\nabla V_i\rangle \tag{22}$$

$$p_i = p_i + \Delta p_i = p_i + \Delta r_i\cdot\langle\nabla p_i\rangle \tag{23}$$

It is necessary to mention that for the present study the ε is equal to 0.05 so as not to have a negative impact on the mixing process and paths.

To have a quantitative analysis, an appropriate criterion for fluid mixing must be defined. Different mixing indices have been defined. In the present study, the mixing index introduced with *Asmar et al.* [32] is applied. They applied their model with a Discrete Element Model (DEM). Because of Particle-based method, the SPH is similar to the DEM. So, *Asmar et al.*'s mixing index can be a proper mixing index for investigation of the SPH mixing modeling.

$$MI_i = \left(MI_{x_i} + MI_{y_i}\right)/2 \tag{24}$$

where $MI_x$is

$$MI_{x_i} = \left(\frac{\sum_{j=1}^{n}(x_j - x_{ref})}{n}\right)\Big/\left(\frac{\sum_{k=1}^{N}(x_k - x_{ref})}{N}\right) \tag{25}$$

where *n* and *N* are respectively the number of particles type i and the total number of the particles. MI_y is also similarly calculated. Although this is a simple method, it usually gives a proper indication of mixing. In a system with two types of particles, $MI = 1$ indicates that particles of type *i* are completely mixed.

Another issue that is addressed in the present study is the resistance of the fluid to the movement of the mixing blades. For this, the resistance torque is calculated as follows:

$$M_r = \int_A r\times((\tau - pI)\cdot n_w)dA, \tag{26}$$

This integral is simply transformed into a summation on the rigid particles of the blades:

$$M_r = \sum_{j=1}^{N_s} r_j\times((\tau - pI)_j\cdot n_{w_j}dA_j, \tag{26}$$

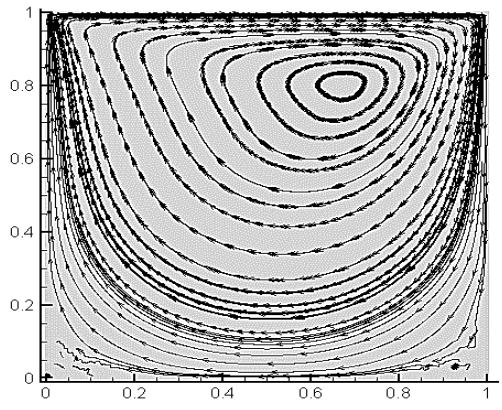

Fig. 1: Stream line for the lid driven cavity for the case Re=100, Bn=1.

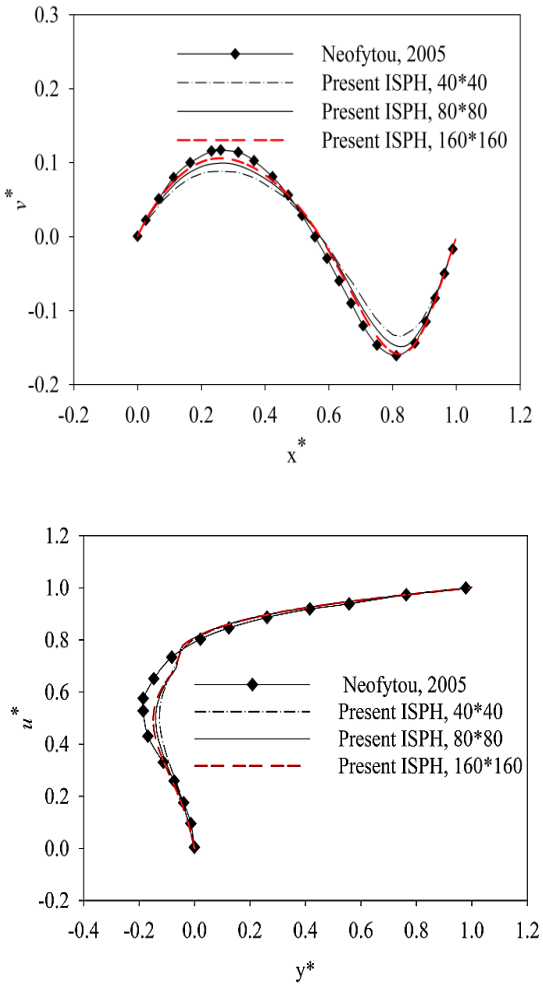

Fig. 2: vertical and horizontal velocity profile of lid driven cavity at the middile horizontal and vertical sections for the case Re=100.

where $\boldsymbol{r}$ is position vector relative to the center of rotation and N_s is the number of solid particles on the desired wall.

Validation

This section deals with the validation of computational code. The problem considered here is the lid-driven cavity containing the Bingham fluid. Bingham number $Bn = \tau_0 L/(\mu_0 U)$=1.0 and the Reynolds number $Re = \rho UL/\mu_0$=100. The SPH modeling has been performed and the results for the streamlines inside the cavity are shown in Fig. 1.

One of the famous benchmarks for this problem is the results presented by Neofytou [39]. In Fig. 2, in comparison with the Neofytou [39], the vertical and horizontal velocity profiles are plotted respectively on the horizontal and vertical middle lines of the cavity. As shown there is a good agreement between the present results and those reported by Neofytou [39]. In this figure, also the effect of particles number on the convergence has been shown. As indicated, the accuracy increases by increasing the number of particles.

RESULTS AND DISCUSION

Mixers can generally be divided into two types of static mixers and dynamic mixers. The static type has no moving parts [40]. But active or dynamic mixers usually increase the mixing rate by one or more moving components. In this study, two types of shear and blender are modeled and discussed.

Shear mixer

In the present study, a rotary 2-D mixer is considered for simulation. It is assumed that the mixer consists of two coaxial cylinders rotating in opposite directions. The cross-section of the mixer is shown in Fig. 3.

The mixer considered is categorized into the shear mixers. In the shear mixers, usually, the velocity difference of the fluid layers due to the formation of shear flow causes the fluid to mix. The shear mixers chamber is usually circular. The shear mixers usually contain a rotary system. In fact, the rotary system creates the shear flow in the mixer. The shear mixers widely are used for mixing of the cement pastes. As mentioned before, the cement pastes can act like a Bingham fluid.

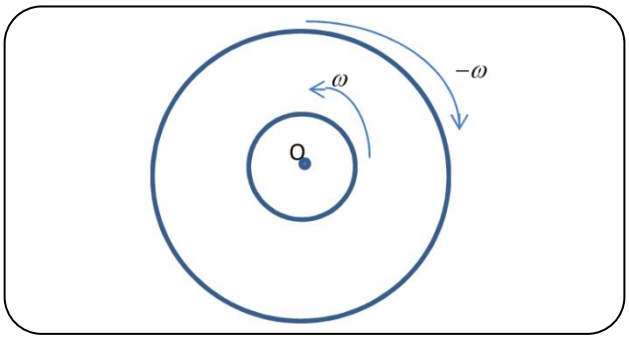

Fig. 3: the cross section of the shear mixer considered for simulation and investigation.

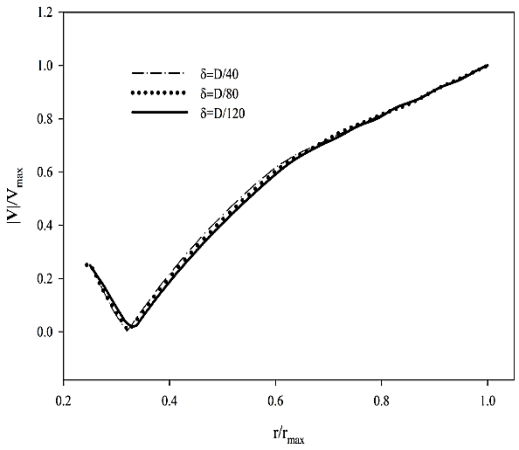

Fig. 4: Effect of particle size on the accuracy for the case Re=14.

The cement paste plastic viscosity is $\mu_0 = 6.4$ Pa.s, yield stress is $\tau_0 = 6.0\ Pa$ and the density of the fluid is $\rho = 2400\ \mathrm{kg/m^3}$. These data are an intermediate value in the range of data presented in the studies of *Lee* and *Choi* [28] and *Li et al.* [29]. Reynolds number is defined as follow:

$$\mathrm{Re} = \frac{\rho V_{max} D}{\mu_0} \qquad (26)$$

where D is the outer dimeter of the mixer and $V_{max}$is the maximum velocity usually recorded at the outer diameter of the mixer. To determine the mixing paths, the fluid in the mixing tank is separated into two different colors.

The effect of the particle size on the accuracy has been investigated by three cases; δ=*D*/40, δ=*D*/80, and δ=*D*/120. The velocity profiles in the mixer chamber for these three cases are plotted in Fig. 4. As indicated, the results are converged and the particle size δ=D/80 is selected for simulations in the present study.

In the first case, the mixing process for Re=14 is examined. For this purpose, the particle distribution contour at different times is plotted in Fig. 5.

It is quite clear that over time, ($t^*=t\times\omega$ >30) the area inside the mixer splits into two areas; the thoroughly mixed area near the inner shell and the non-mixed area near the outer shell. This figure shows that the passage of time will not eliminate the unmixed zone. Further study by the authors shows that the cause of these two regions is the dual behavior of Bingham fluid (behavior before yield stress and after yield stress). Therefore, in order to eliminate the unmixed zone, the strain rate must be increased. So, in this paper, the effect of the Reynolds number, which will be shown to be an influential parameter on the mixing rate in Bingham fluid, is investigated.

In Fig. 6, the distribution of the particles inside the mixer is shown at $t^*=t\times\omega= 80$ for five different Reynolds numbers: Re=14, Re=28, Re=56, Re=112 and Re=224.

For the case Re=14, the fluid near the inner wall is completely mixed and from a certain radial distance to the outer shell an unmixed region appears. By increasing the Reynolds number, a greater radius of mixer is involved in fluid mixing and the unmixed region is reduced. Approximately, at Re = 224 the radius of the mixed region is equal to the mixer radius. The mixing phenomenon extends to all the surface of the mixer, and the intertwined spiral layers of the two fluids are observed throughout the mixer surface. But this is a qualitative study. To have a quantitative comparison index, the mixing index is calculated.

To calculate this index, the fluid in the mixing tank is separated into two different colors. Now with this color separation, the mixing index can be evaluated for each component (each color) according to Eq. (25). Each color is considered a component. The time variations of the mixing index for these five cases are shown in Fig. 7.

There is a spiral mixing path inside the tank. As the tank of mixer rotates, the non-mixing zones also move frequently, producing a periodic motion in the reservoir. So, the variation of the mixing index has a periodic form. But as the Reynolds number increases, the amplitude of the fluctuations declines considerably. The variation of fluctuations for Reynolds number 14 is about 0.5 (between

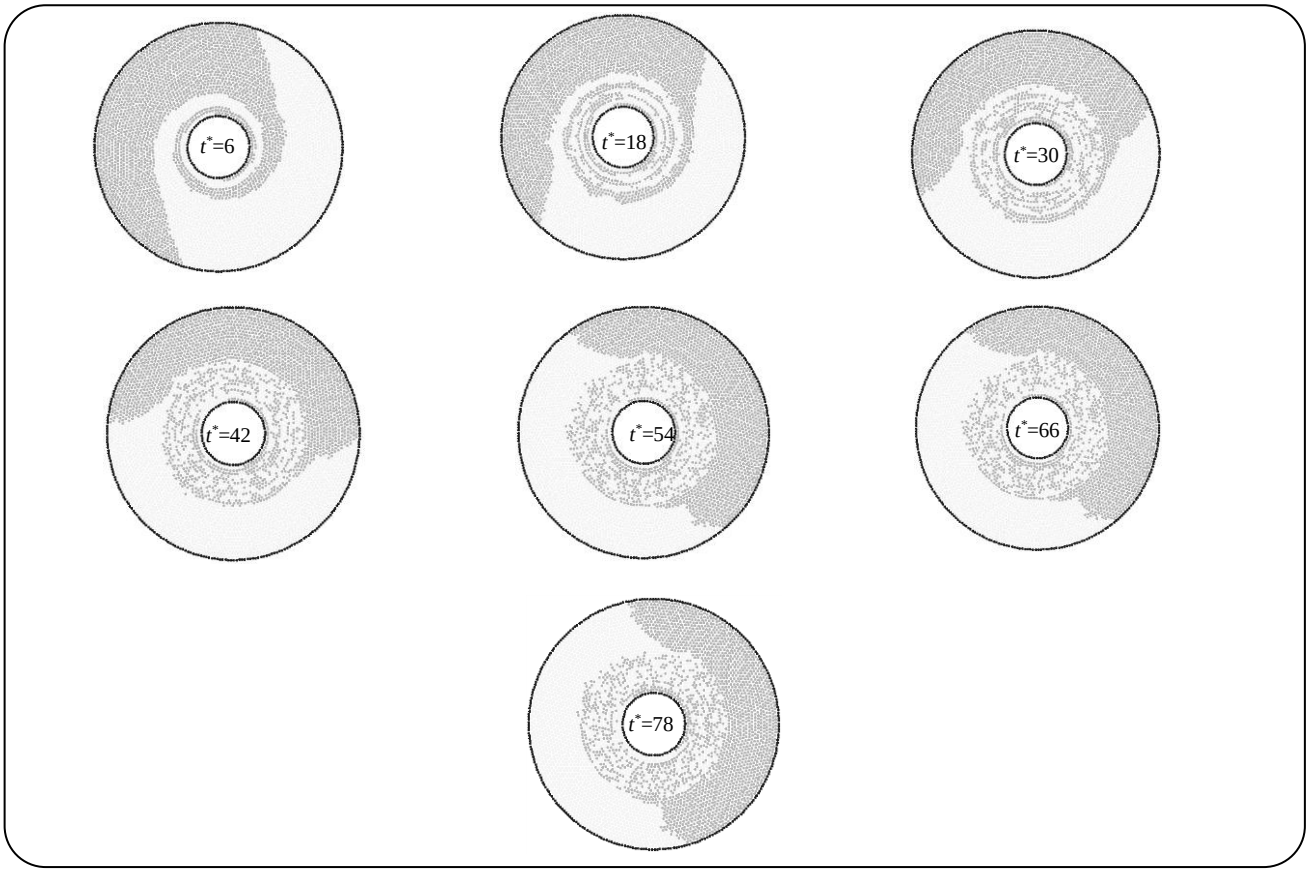

Fig. 5: Distribution of particles inside the shear mixer for Reynolds number 14.

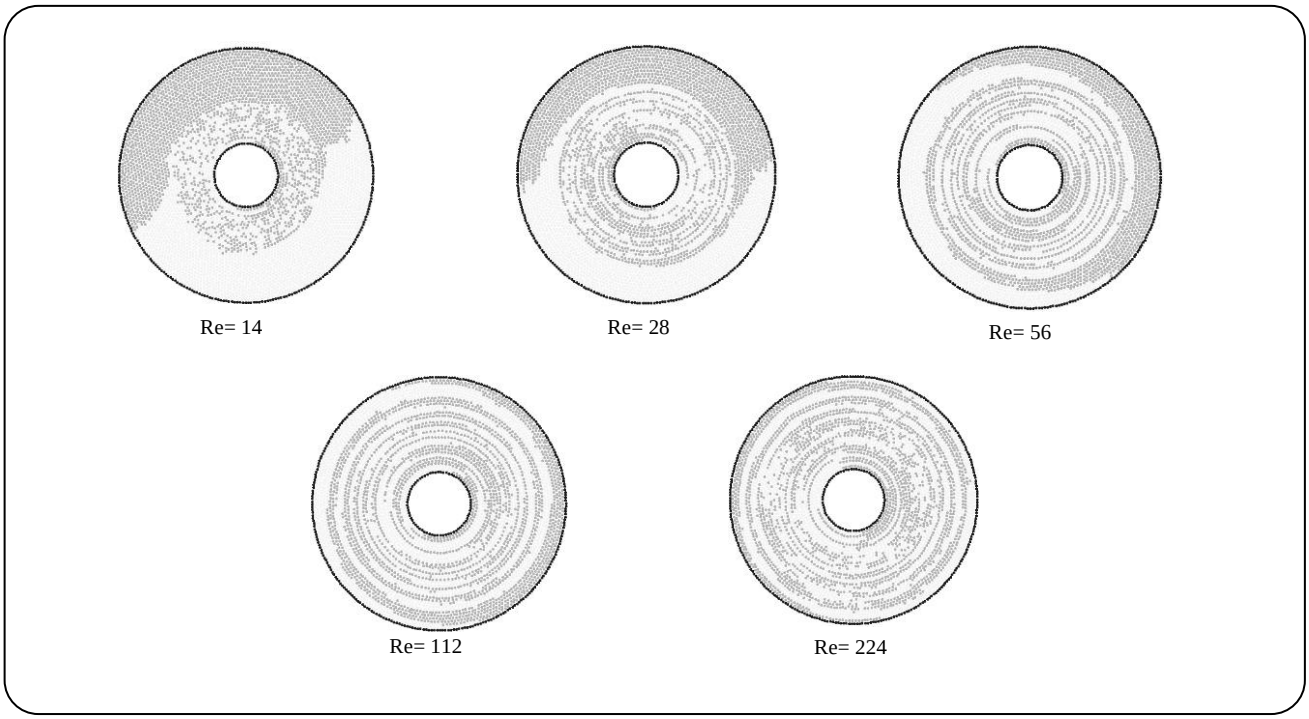

Fig. 6: The effect of Reynolds number on the mixing; particle distribution in the mixer for five different Reynolds number at t*=80.

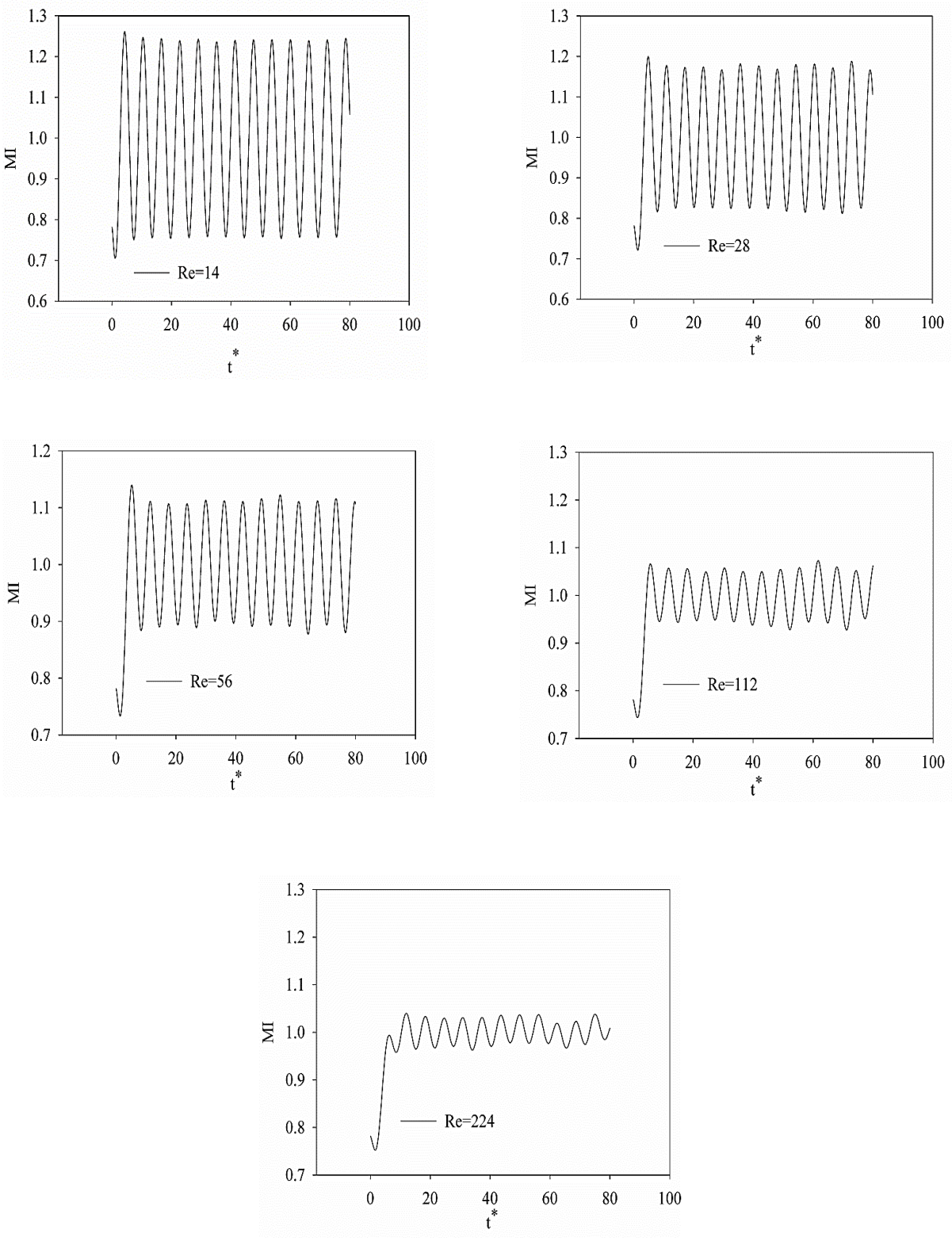

Fig. 7: Time variation of mixing index for five different Reynolds number.

0.75 and 1.25) and for Reynolds number 224 is about 0.1 between (0.95 to1.05). This represents an 80% decrease in the mixing index in increasing the Reynolds number from 14 to 224. This indicates a significant increase in mixing with increasing Reynolds number.

In Fig. 8, the variation of the radius of the mixed region rather than the outer wall radius ($r^*=r_{mix}/R_{out}$) versus the Reynolds number is plotted. In this figure the results of the same state but in the Newtonian state ($\mu_{Newtonian} = \mu_0$) are also shown. The result is a nonlinear curve showing that with increasing Reynolds number the curve slope is decreasing although the mixing area increases. The results also show that the unmixed area in the Bingham fluid case is much larger than the Newtonian fluid case.

The main reason for this behavior relates to the inherent nature of the Bingham fluid. Bingham fluid has a dual behavior; it acts as a solid and also it can act as a fluid. These conditions are characterized by yield stress. This type of fluid requires a certain amount of initial stress to flow. A shear stress threshold is defined for them that no flow is seen before the shear stress reaches this threshold, and then the fluid begins to flow. Now with this explanation, we can justify the Bingham fluid behavior in this phenomenon; in the non-Newtonian Bingham fluid mixing phenomenon, some energy is passed over the yield stress value. Thus, by increasing the Reynolds number, the kinetic energy of the particles required for complete mixing is provided.

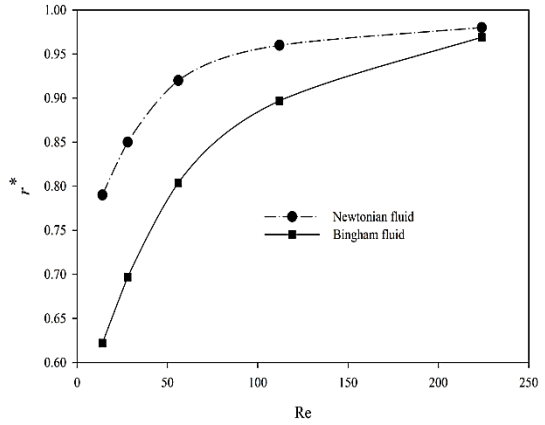

Fig. 8: The variation of the radius of the mixed region rather than the outer wall radius versus the Reynolds number.

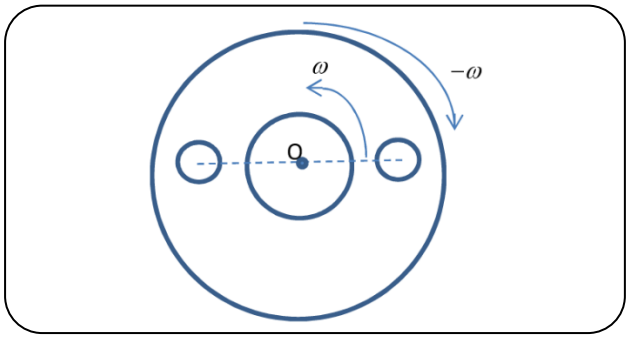

Fig. 9: the cross section of the mechanism considered for blending the cement paste.

Mixing due to blending

In the shear mechanism which was investigated in the previous section, the particles of two fluids are distributed along with the shear layers. However, the two particles are not completely mixed. To have a more homogeneous distribution of the particles in the mixer, a blending mechanism which its cross-section is shown in Fig. 9 is considered and investigated.

To follow the fluid mixing paths, the particle distribution at different times are extracted and evaluated at constant Reynolds number Re=224 (the maximum Reynolds number examined in the previous section). The results are shown in Fig. 10. As can be seen in the figure, the shear layers of the mix have disappeared and fluid mass movement is observed instead. In fact, it seems that the fluid moves massively and collectively in the tank of the mixer which is clearly observed in particle distribution of times t*=4.8 and t*=14.4. The scattering occurs very slowly and gradually. The unmixed regions are distributed almost symmetrically on the two sides of the internal moving set. Unmixed region areas become smaller and smaller over time. It seems that the shear mixing mechanism is formed near the outer wall.

In Fig. 11, the time variation of the mixing index for this case has been plotted. The presence of different mixing mechanisms in the mixer causes irregular behavior in this diagram. However, the trend diagram shows that gradually the mixing index tends to 1, indicating almost complete mixing.

Fluid flow resistance

To better compare the performance of shear and blender mixers, this section compares the resistance of the fluid to the movement of the mixer. For example, the result obtained from equation (27) for Reynolds number 224 for blending mixing is shown in Fig. 12.

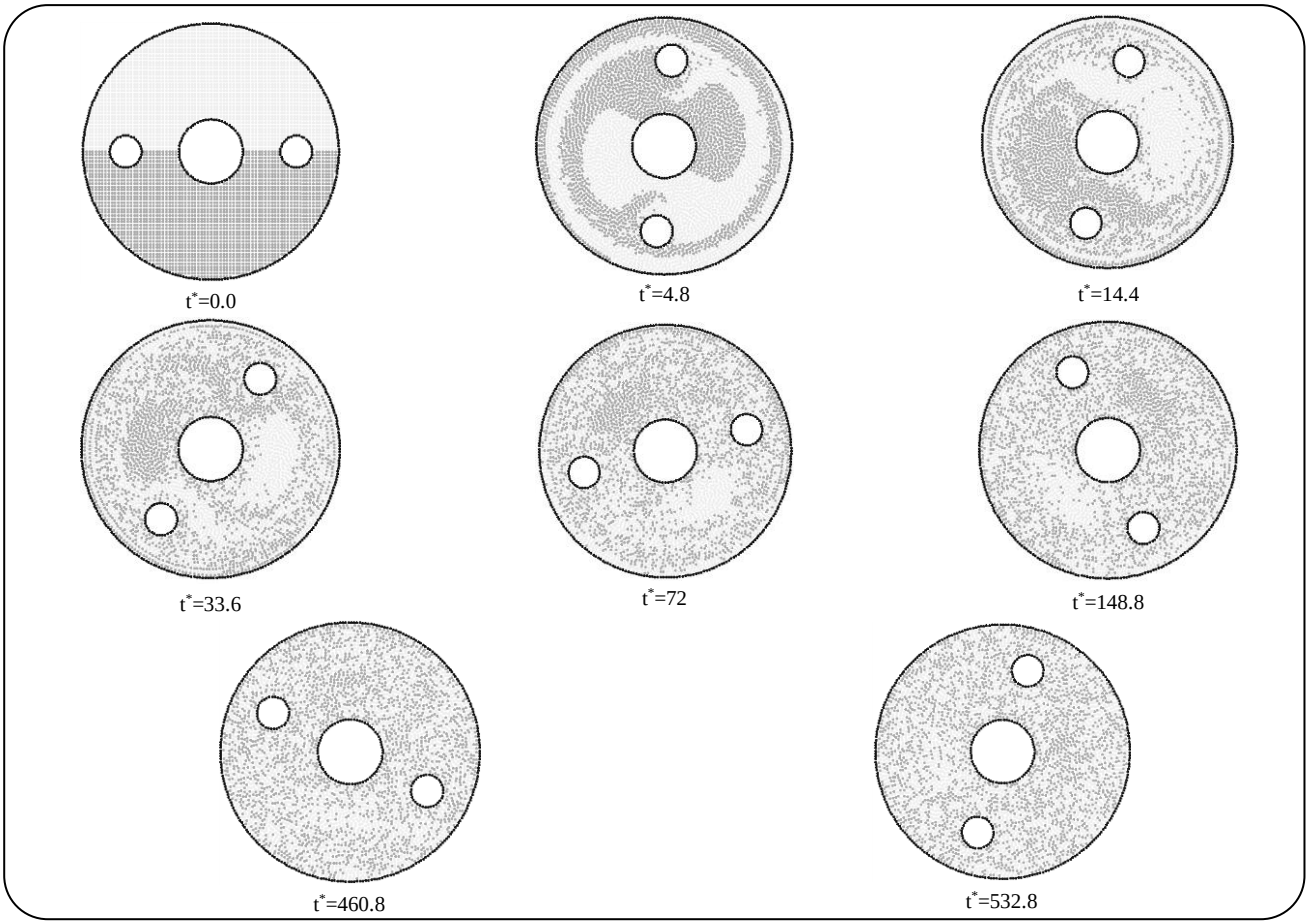

Fig. 10: The particle distribution at different times for the case Re=224.

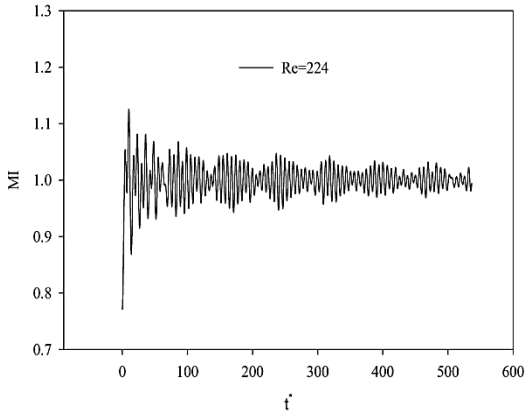

Fig. 11: The time variation of mixing index for the case Re=224.

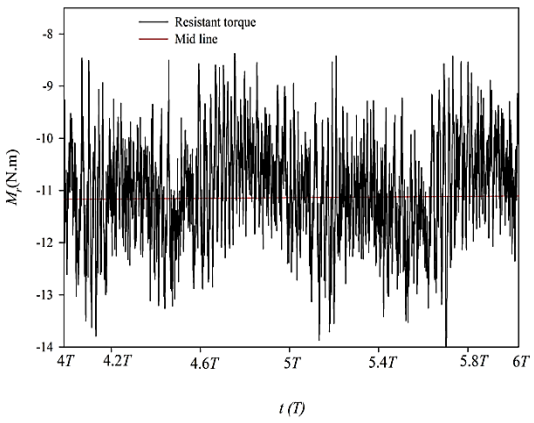

Fig. 12: Time variations of the resistive torque for the blender mixer for the case Re=224.

In this figure, the resistive torque applied by the fluid to the blender during the period of the blender's rotation is plotted. Part of the sharp fluctuations in torque is related to changes in fluid behavior due to strain rates, and part is related to fluctuations in pressure inside the mixer. In this figure, the average torque value is also shown, which is a good criterion for comparison.

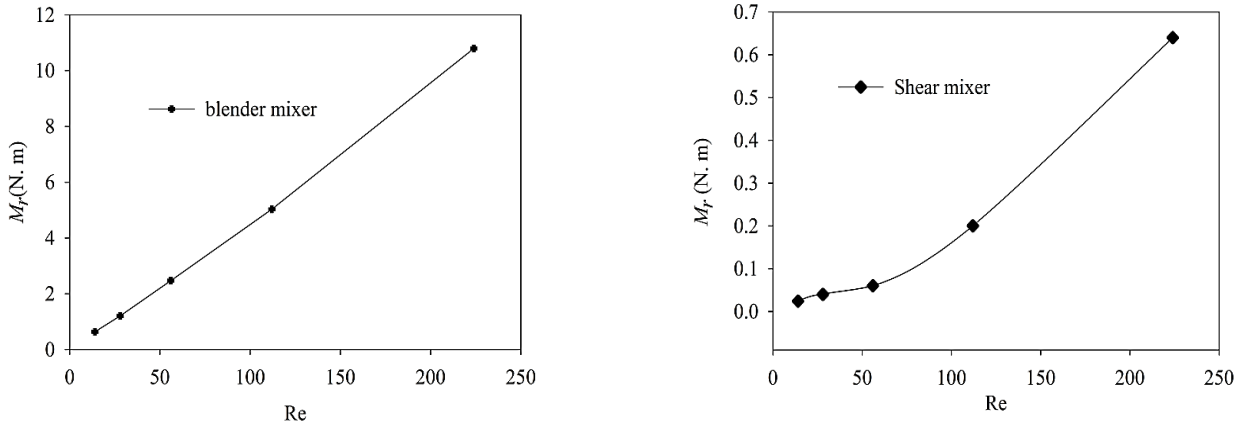

Fig. 13: The resistive torque vs. Reynolds number for a: blender mixer, and b: shear mixer.

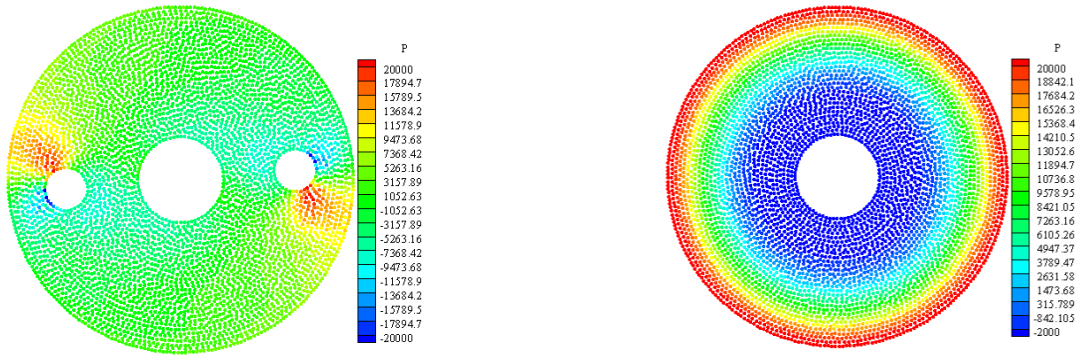

Fig. 14: The pressure contour for the blender mixer (left) and shear mixer (right).

Fig. 13a shows the variation of the average torque versus the Reynolds number for the blending mode. In contrast, Figure 13b shows the torque variations versus the Reynolds number for the shear mixing mode.

As can be seen, the order of resistant torque in the shear mode is much lower than in the blending mode. For a closer look at the cause of the difference, the pressure contour for both states is plotted in the Reynolds number 224 in Figure 14. As you can see, in the blending mode (left figure), around the planetary cylinders, in front of the cylinder, there is a high-pressure zone, and behind the cylinder, there is a low-pressure zone (wake). This pressure difference indicates the presence of pressure drag in front of the planetary cylinders. However, as shown in Figure 14, for a shear mixer, pressure changes occur only in the radius direction and pressure changes in the angle direction are negligible. For this reason, drag force can be considered as only frictional drag. So, the significant difference in the amount of resistive torque in the two modes is related to the difference in the nature of the two flows. In shear flow, the amount of drag is mostly related to frictional drag, while in blending mode it is related to pressure drag. Since the fluid-resistant torque is directly related to electrical power consumption, the power consumption of shear mixers is far less than the power consumption of blender mixers.

Figure 15 shows the flow lines of both types of mixers (the left figure is the blender mixer and the right figure is the shear mixer). Before, *Shuiping et al.* [30] showed that the mixer produced strong vortices under the action of the spiral blade combined the nozzles. Here, too, these vortices are clearly visible in the blender mixer model. In this model, two small vortices are formed between the two middle circular blades (planetary blades) and the outer shell. Two larger vortices also form between the two planetary fins (approximately on a fixed radius from

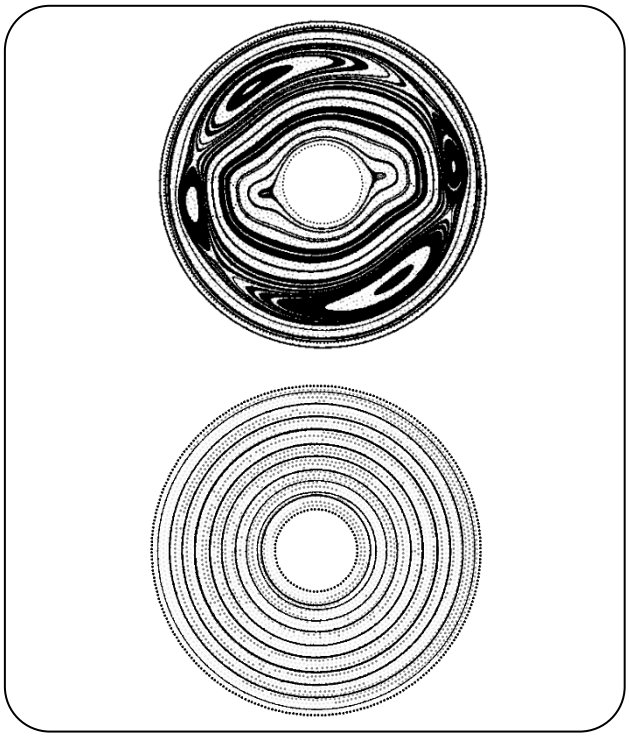

Fig. 15: Stream line for the blender mixer (left figure) and shear mixer (right figure).

the center of the mixer). It should be noted that these vortices move with the rotation of the blades. This is why mass motion is formed in this mixer. In the shear model, the flow lines are concentric circles that form between the inner blade and the outer shell which indicates the formation of shear flow.

CONCLUSIONS

In the present study, a robust Incompressible SPH method has been developed and used to model the mixing phenomenon in a rotary cement paste mixer. The cement paste is assumed to be a Bingham fluid. The method validated against a famous benchmark and then is used to simulate the cement paste mixer in two types; shear mixer and blender. An appropriate mixing index that was previously applied to the discrete element method was successfully implemented for the ISPH method. In the present study, both shear and blender mixers are modeled and evaluated by this index. These mixers were modeled and evaluated based on Reynolds number. In the shear model, it was observed that the mixing phenomenon is divided into mixed and unmixed regions. In the mixed area, the shear layers create circular mixing paths. As the Reynolds number increases, these circular paths become wider in the non-mixed region (As the Reynolds number increases, the non-mixed area becomes smaller). In blender mixers, the mixing rate is expected to increase with the multiplicity of vortices formed. But the coordinated motion of the vortices with the blades causes a fluid mass to move which slowed down the mixing process. Also, the fluid resistant torque against of the blades motion was calculated. The results showed that the resistance of the fluid to the movement of the blade in the blender mixer is much higher (more than fifteen times).

Received : Aug. 23, 2021 ; Accepted : Nov. 13, 2021

REFERENCES

[1] Zhang X., Ahmadi G., Eulerian–Lagrangian Simulations of Liquid–Gas–Solid Flows in Three-Phase Slurry Reactors, *Chem. Eng. Sci.*, **60**: 5089-5104 (2005).

[2] Gingold R.A., Monaghan J.J., Smoothed Particle Hydrodynamics: Theory and Application to Non-Spherical Stars, *Mon. Not. R. Astron. Soc.*, **181**: 375-389 (1977).

[3] Lucy L.B., A Numerical Approach to the Testing of Fusion Process, *Astron. J.*, **88**: 1013-1024 (1977).

[4] Rafiee A., Manzari M.T., Hosseini M., An Incompressible SPH Method For Simulation of Unsteady Viscoelastic Free-Surface Flows, *Int. J. Nonlin. Mech.*, **42**: 1210–1223 (2007).

[5] Kiara A., Hendrickson K., Yue D.K.P., SPH for Incompressible Free-Surface Flows. Part I: Error Analysis of the Basic Assumptions, *Comput. Fluids*, **86**: 611-624 (2013).

[6] Kiara A., Hendrickson K., Yue D.K.P., SPH for Incompressible Free-Surface Flows. Part II: Performance of a Modified SPH Method, *Comput. Fluids*, **86**: 510-536 (2013).

[7] Jiang T., Ouyang J., Li Q., Ren J., Yang B., A Corrected Smoothed Particle Hydrodynamics Method for Solving Transient Viscoelastic Fluid Flows, *Appl. Math. Model.*, **35**: 3833-3853 (2011).

[8] Cleary P.W., Modeling Confined Multi-Material Heat and Mass Flows Using SPH, *Appl. Math. Model.*, **22**: 981–993 (1998).

[9] Shadloo M.S., Zainali A., Yildiz M., Simulation of Single Mode Rayleigh–Taylor Instability by SPH Method, *Comput. Mech.*, **51(5)**: 699-715 (2013).

[10] Liu X., Xu H., Shao S., Lin P., An Improved Incompressible SPH Model for Simulation of Wave–Structure Interaction, *Comput. Fluids*, **71**: 113-123 (2013).
[11] Rafiee A., Thiagarajan K.P., An SPH Projection Method for Simulating Fluid-Hypoelastic Structure Interaction, *Comput. Methods Appl. Mech. Eng.*, **198**: 2785–2795 (2009).
[12] Hashemi M.R., Fatehi R., Manzari M.T., A Modified SPH Method for Simulating Motion of Rigid Bodies in Newtonian Fluid Flows, *Int. J. Nonlin. Mech.*, **47**: 626-638 (2012).
[13] Hashemi, M.R., Fatehi, R., Manzari, M.T., SPH Simulation of Interacting Solid Bodies Suspended in A Shear Flow of an Oldroyd-B fluid, *J. Non-Newton. Fluid.*, **166**:1239-1252 (2011).
[14] Lai, J., Wang, H., Yang, H., Zheng, X., Wang, Q., Dynamic Properties and SPH Simulation of Functionally Graded Cementitious Composite Subjected to Repeated Penetration, *Constr. Build Mater.*, **146**: 54-65 (2017).
[15] Cao G., Li Z., Xu Z., A SPH Simulation Method For Opening Flow of Fresh Concrete Considering Boundary Restraint, *Constr. Build Mater*, **198**: 379-389 (2019).
[16] Lenaerts T., Dutré P., Mixing Fluids and Granular Materials, *Comput. Graph. Forum.*, **28**: 213-218 (2009).
[17] Robinson M., ClearyP., Monaghan J., Analysis of Mixing in a Twin Cam Mixer Using Smoothed Particle Hydrodynamics, *AIChE Journal*, **54**: 1987-1998 (2008).
[18] Orthmann J., Kolb A., Temporal Blending for Adaptive SPH, *Comput. Graph. Forum*, **31**: 1-12 (2012).
[19] Shamsoddini R., Sefid M., Fatehi R., ISPH Modelling and Analysis of Fluid Mixing in a Microchannel with an Oscillating or a Rotating Stirrer, *Eng. Appl. Comp. Fluid.*, **8(2)**: 289-298 (2014).
[20] Shamsoddini R., Sefid M., Fatehi R., Lagrangian Simulation and Analysis of the Micromixing Phenomena in a Cylindrical Paddle Mixer Using a Modified Weakly Compressible, *Asia Pac. J. Chem. Eng.*, **15(1)**: 1-10 (2015).
[21] Shamsoddini R., Sefid M., Lagrangian Simulation and Analysis of the Power-Law Fluid Mixing in the Two-Blade Circular Mixers Using a Modified WCSPH Method, *Pol. J. Chem. Tech.*, **17(2)**:1-10 (2015).
[22] Shamsoddini R., Numerical Investigation of Fluid Mixing in a Micro-Channel Mixer with Two Rotating Stirrers by Using the Incompressible SPH Method, *Iran. J. Chem. Chem. Eng. (IJCCE)*, **36(5)**: 173-183 (2017).
[23] Shamsoddini R, Aminizadeh N., Incompressible Smoothed Particle Hydrodynamics Modeling and Investigation of Fluid Mixing in a Rectangular Stirred Tank with Free Surface, *Chem. Eng. Commun.*, **204(5)**: 563–572 (2017).
[24] Shamsoddini R., Incompressible SPH Modeling of Rotary Micropump Mixers, *Int. J. Comp. Meth.* **15(4)**: 1850019 (2018).
[25] Abdolahzadeh M., Tayebi A., Omidvar P., Mixing Process of Two-Phase Non-Newtonian Fluids in 2D Using Smoothed Particle Hydrodynamics, *Comput. Math. Appl.*, **78(1)**: 110-122 (2019).
[26] Bentaieb N., Benarima Z., Belaadi S., Calorimetric and Thermal Analysis Studies on the Influence of Coal on Cement Paste Hydration, *Iran. J. Chem. Chem. Eng. (IJCCE)*, **39(6)**: 237-244 (2020)
[27] Abolpour B., Afsahi M.M., Hosseini S.G., Statistical Analysis of the Effective Factors on the 28 Days Compressive Strength and Setting Time of the Concrete, *J. Adv. Res.*, **6(5)**: 699-709 (2015).
[28] Lee DK., Choi M.S., Standard Reference Materials for Cement Paste: Part II-Determination of Mixing Ratios, *Materials*, **11**: 861 (2018).
[29] Li D., Wang D., Ren C., Rui Y. Investigation of Rheological Properties of Fresh Cement Paste Containing Ultrafine Circulating Fluidized Bed Fly Ash, *Constr Build Mater.*, **188(10)**: 1007-1013 (2018).
[30] Shuiping L., Xiaotian L., Lugang S. Simulation of the Flow Field of Cement Mixer Based on Numerical Methods, *Adv. Syst. Sci. Appl.*, **11(3-4)**: 315-321 (2011).
[31] Beccati N., Ferrari C., Bonanno A., Balestra M., Calibration of a CFD Discharge Process Model of an Off-Road Self-Loading Concrete Mixer, *J Braz. Soc. Mech. Sci. Eng.*, **41**: 76 (2019).
[32] Asmar B., Langston P., Matchett A., A Generalised Mixing Index in Distinct Element Method Simulation of Vibrated Particulate Beds, *Granul. Matter*, **4**: 129–138 (2002).

[33] Capone T., Panizzo A., Cecioni C., Dalrymple R.A., Accuracy and stability of Numerical Schemes in SPH, Proceedings of the Workshop "SPHERIC - Smoothed Particle Hydrodynamics European Research Interest Community, 156 (2007).

[34] Bonet J., Lok T.S., Variational and Momentum Preservation Aspects of Smooth Particle Hydrodynamic Formulation, *Comput. Methods Appl. Mech. Eng.*, **180**: 97-115 (1999).

[35] Jayasree C., Murali Krishnan J., Gettu R., Influence of Superplasticizer on the Non-Newtonian Characteristics of Cement Paste, *Mater. Struct.*, **44**: 929–942 (2011).

[36] Papanastasiou T.C., Flows of Materials with Yield., *J. Rheol.*, **31**: 385–404 (1987).

[37] Shadloo M.S., Zainali A., Sadek S.H., Yildiz M., Improved Incompressible Smoothed Particle Hydrodynamics Method for Simulating Flow Around Bluff Bodies, *Comput. Methods Appl. Mech. Eng.*, **200**: 1008–1020 (2011).

[38] Sefid M., Fatehi R., Shamsoddini R., A Modified Smoothed Particle Hydrodynamics Scheme to Model the Stationary and Moving Boundary Problems for Newtonian Fluid Flows, *ASME J. Fluids Eng.*, **137(3)**: 03120/1-9 (2015).

[39] Neofytou P., A 3rd order upwind finite volume method for generalised Newtonian fluid flows, *Adv. Eng. Soft*, **36 (10)**: 664-680 (2005).

[40] Rajamanickam A., Krishnaswamy B., Design and Development of Mathematical Model for Static Mixer, *Iran. J. Chem. Chem. Eng. (IJCCE)*, **35(1)**: 109-116 (2016).